

Supporting Information

## Double Charge Transfer Processes Enable Green Multiple Resonance Induced Thermally Activated Delayed Fluorescence Emitter for Efficient Narrowband OLED

Xu-Feng Luo\*,<sup>a,b</sup> Liangjun Shen,<sup>a</sup> Jun-Yi Wang,<sup>a</sup> Xunwen Xiao\*,<sup>a</sup>

<sup>a</sup>College of Material Science and Chemical Engineering, Ningbo University of Technology, 201 Fenghua Road, Ningbo 315211, P. R. China.

E-mail: [luoxf@nbut.edu.cn](mailto:luoxf@nbut.edu.cn), [xunwenxiao@nbut.edu.cn](mailto:xunwenxiao@nbut.edu.cn)

<sup>b</sup>State Key Laboratory of Coordination Chemistry, School of Chemistry and Chemical Engineering, Nanjing University, Nanjing 210093, P. R. China

### 1. Instrumentation and materials.

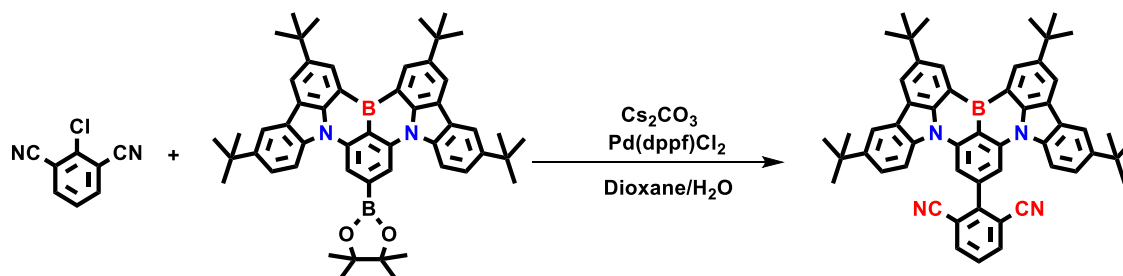
All of the reagent and solvent were obtained from commercial sources and directly used without any further purification. <sup>1</sup>H and <sup>13</sup>C NMR spectra were measured on a Bruker ARX 500 NMR spectrometer and reported as parts per million (ppm) from the internal standard TMS. High-resolution mass spectra were recorded on a MICROTOF-Q III instrument. Absorption and photoluminescence spectra were measured on a Shimadzu UV-3100 and a Hitachi F-4600 photoluminescence spectrophotometer, respectively. Cyclic voltammetry measurements were conducted on a MPI-A multifunctional electrochemical luminescent system (Xi'an Remex Analytical Instrument Ltd. Co., China) at room temperature with a polished Pt plate as the working electrode, platinum thread as the counter electrode and Ag-AgNO<sub>3</sub> (0.1 M) in CH<sub>3</sub>CN as the reference electrode, *tetra-n*-butylammonium hexafluorophosphate (0.1 M) was used as the supporting electrolyte, respectively, using Fc<sup>+</sup>/Fc as the internal standard, the scan rate was 0.1 V/s. The absolute photoluminescence quantum yields via an integrating sphere and the decay lifetimes of the compounds were measured with HORIBA Fluorolog-3 fluorescence spectrometer. The thermogravimetric analysis (TGA) curve was performed on a Pyris 1 DSC under nitrogen at a heating rate of 10 °C min<sup>-1</sup>. The ground state calculations are based on optimized structure using Gaussian 09 by density functional theory (DFT) using the B3LYP functional with the 6-31G(d,p) basis set; excited state calculations and Van der Waals surface wrapped with electrostatic potential (ESP) and reduced density gradient (RDG) analysis were conducted by time-dependent density functional theory (TD-DFT) with B3LYP functional with the 6-31G(d,p) basis set.

Indium-tin-oxide (ITO) coated glass with a sheet resistance of 10 Ω sq<sup>-1</sup> was used as the anode substrate. Prior to film deposition, patterned ITO substrates were cleaned with detergent, washed by de-ionized water, dried and treated with oxygen plasma for 10 minutes at a pressure of 10 Pa to enhance the surface work function of ITO anode (from 4.7 to 5.1 eV). All the organic layers were

deposited with the rate of 0.1 nm/s under high vacuum ( $\leq 9 \times 10^{-5}$  Pa). The doped layers were prepared by co-evaporating dopant and host material from two individual sources, and the doping concentrations were modulated by controlling the evaporation rate of dopant. LiF and Al were deposited in another vacuum chamber ( $\leq 1.0 \times 10^{-4}$  Pa) with the rates of 0.01 and 1 nm/s, respectively, without being exposed to the atmosphere. The thicknesses of these deposited layers and the evaporation rate of individual materials were monitored in vacuum with quartz crystal monitors. A shadow mask was used to define the cathode and to make ten emitting dots (with the active area of 10 mm<sup>2</sup>) on each substrate. Device performances were measured via using a programmable Keithley source measurement unit (Keithley 2400 and Keithley 2000) with a silicon photodiode. The EL spectra were measured with a Hitachi F-4600 spectrophotometer. Based on the uncorrected EL fluorescence spectra, the Commission International e de l'Eclairage (CIE) coordinates were calculated using the test program of Spectra scan PR650 spectrophotometer. The EQE of EL devices were calculated based on the photo energy measured by the photodiode, the EL spectrum, and the current pass through the OLED.

## 2. Experimental section

All other of the reagents and solvents were obtained from commercial sources and directly used without any further purification. The synthesis details of Scheme S1 are described in the following:



**Scheme S1.** The synthetic route of BNDCN.

### 2.1 Preparation procedure for BNDCN

2-chloroisophthalonitrile (0.2 g, 1.2 mmol), DtCzB-Bpin (1.1 g, 1.4 mmol) and Cs<sub>2</sub>CO<sub>3</sub> (0.6 g, 1.8 mmol) were dissolved in dioxane/H<sub>2</sub>O (20 mL) at room temperature. The mixture was stirred at 100 °C for 8 h. After cooling to room temperature, the reaction mixture was poured into a large amount of water. The product was extracted with dichloromethane, and the combined organic layer was dried over anhydrous MgSO<sub>4</sub>. After evaporation, the product was purified by column chromatography (PE/DCM= 7/1, v/v) to get the **BNDCN** as a yellow solid (0.6 g, yield: 65%). <sup>1</sup>H NMR (500 MHz, CDCl<sub>3</sub>) δ 9.17 (d, *J* = 1.4 Hz, 2H), 8.56 – 8.46 (m, 6H), 8.30 (d, *J* = 1.7 Hz, 2H), 8.16 (d, *J* = 7.9 Hz, 2H), 7.76 (s, 1H), 7.68 (dd, *J* = 8.8, 1.8 Hz, 2H), 1.72 (s, 18H), 1.55 (s, 18H). <sup>13</sup>C NMR (126 MHz, CDCl<sub>3</sub>) δ 149.01 (s), 145.81 (s), 145.17 (s), 144.43 (s),

141.70 (s), 138.27 (d,  $J = 5.4$  Hz), 137.52 (s), 129.92 (s), 128.99 (s), 127.22 (s), 124.70 (s), 123.98 (s), 121.11 (s), 117.41 (s), 116.93 (s), 114.81 (s), 114.05 (s), 108.47 (s), 77.29 (s), 77.04 (s), 76.79 (s), 35.25 (s), 34.84 (s), 32.20 (s), 31.82 (s). HRMS (MALDI-TOF,  $m/z$ ):  $[M]^+$  calcd for  $C_{54}H_{51}BN_4$ , 766.421; found, 766.694.

### 3. NMR spectra

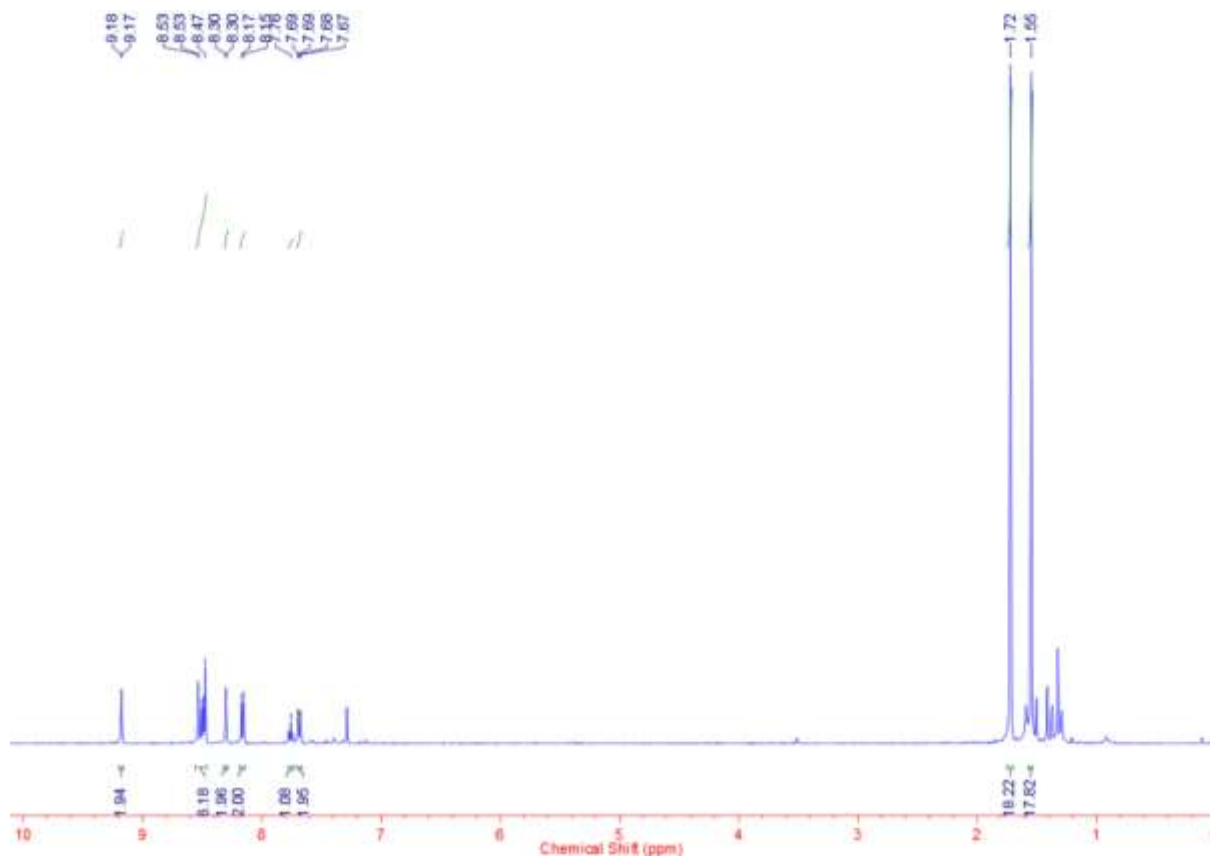


Fig. S1  $^1H$  NMR spectrum of BND CN in  $CDCl_3$ .

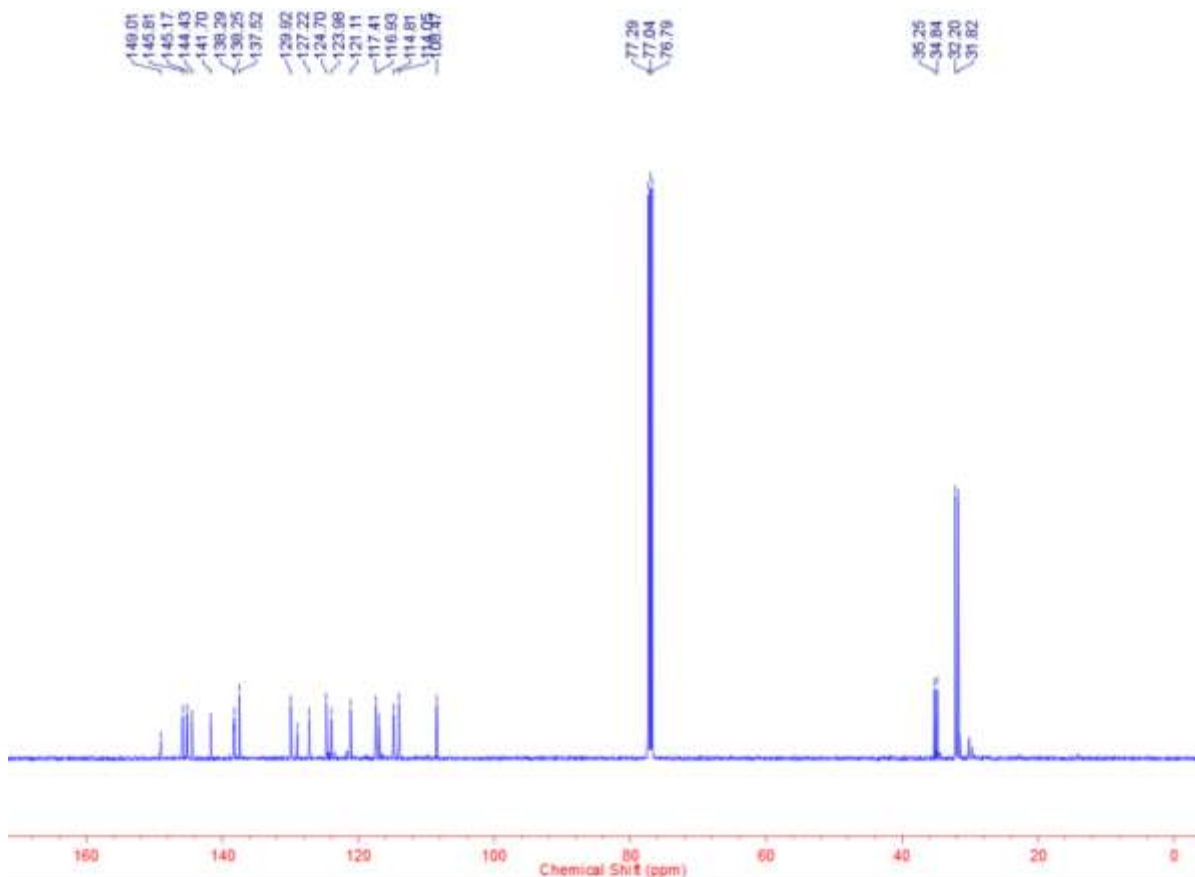


Fig. S2  $^{13}\text{C}$  NMR spectrum of BNDCN in  $\text{CDCl}_3$ .

### 3. Thermal gravimetric analyzer

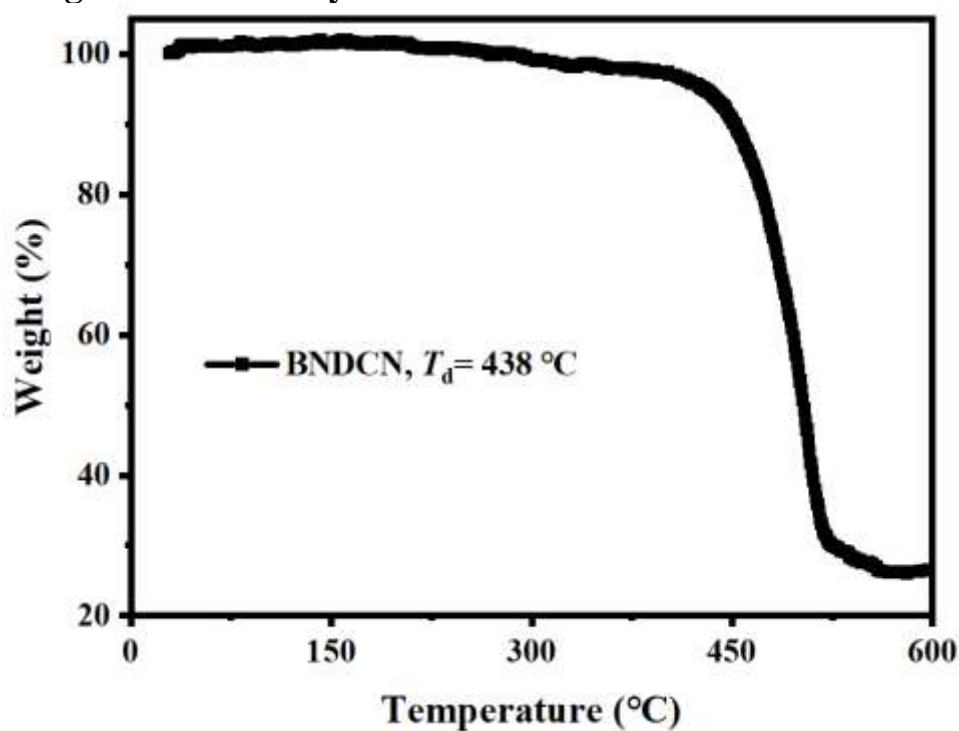


Fig. S3 TGA curve of BNDCN.

## 4. Absorption and emission performance

### 4.1 Photophysical data of BNDCN.

**Table S1.** Photophysical data of the BNDCN.

Compound	$\lambda_{\text{abs}}^{\text{a}}$ [nm]	$\lambda_{\text{PL}}^{\text{b}}$ [nm]	FWHM <sup>c</sup> [nm]	$S_1^{\text{d}}$ [eV]	$T_1^{\text{e}}$ [eV]	$\Delta E_{\text{ST}}^{\text{f}}$ [eV]	$\Phi_{\text{PL}}^{\text{g}}$ [%]	$\tau_{\text{p}}^{\text{h}}$ [ns]	$\tau_{\text{d}}^{\text{h}}$ [μs]	$k_{\text{r}}^{\text{i}}$ [ $10^8 \text{ s}^{-1}$ ]	$k_{\text{ISC}}^{\text{i}}$ [ $10^8 \text{ s}^{-1}$ ]	$k_{\text{RISC}}^{\text{i}}$ [ $10^5 \text{ s}^{-1}$ ]
BNDCN	475	505	27	2.57	2.51	0.06	90	3.2	16.0	1.9	1.3	0.8

<sup>a</sup>Absorption peak at room temperature measured in toluene solution ( $5.0 \times 10^{-5} \text{ M}$ ). <sup>b</sup>Emission peak at room temperature measured in toluene solution ( $5.0 \times 10^{-5} \text{ M}$ ). <sup>c</sup>Full width at half maximum of emission spectrum for PL spectrum. <sup>d</sup>Calculated by the fluorescence spectrum at room temperature. <sup>e</sup>Calculated by the phosphorescence spectrum at 77 K. <sup>f</sup>Estimated by  $S_1$  and  $T_1$ . <sup>g</sup>Absolute photoluminescence quantum yield measured in doped film. <sup>h</sup>prompt decay and delayed fluorescence lifetime in doped film. <sup>i</sup>Rate constant of fluorescence radiative decay ( $S_1 \rightarrow S_0$ ):  $k_{\text{r}} = \Phi_{\text{p}}/\tau_{\text{p}}$ ; Rate constant of ISC ( $S_1 \rightarrow T_1$ ):  $k_{\text{ISC}} = (1 - \Phi_{\text{p}})/\tau_{\text{p}}$ ; Rate constant of RISC ( $T_1 \rightarrow S_1$ ):  $k_{\text{RISC}} = \Phi_{\text{d}}/(k_{\text{ISC}} \cdot \tau_{\text{d}} \cdot \Phi_{\text{p}})$ .

### 4.2 Photoluminescence spectra of BNDCN in various solvents

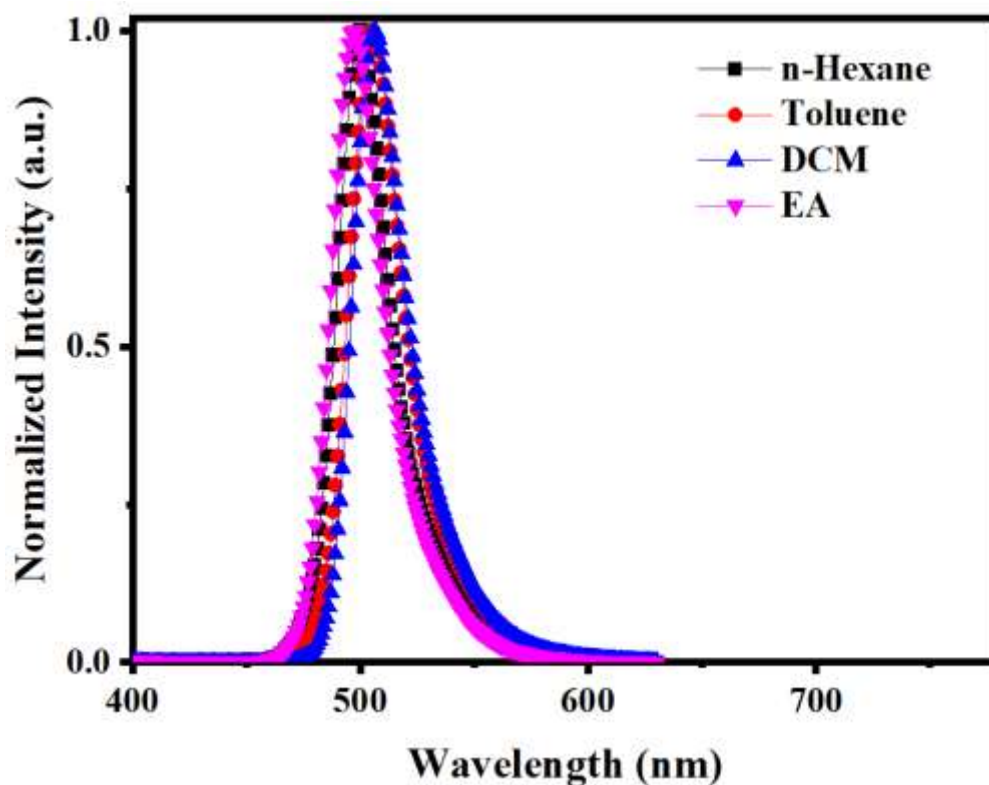


**Fig. S4** Photoluminescence spectra of BNDCN in various solvents.

## 5. Cyclic voltammogram curve

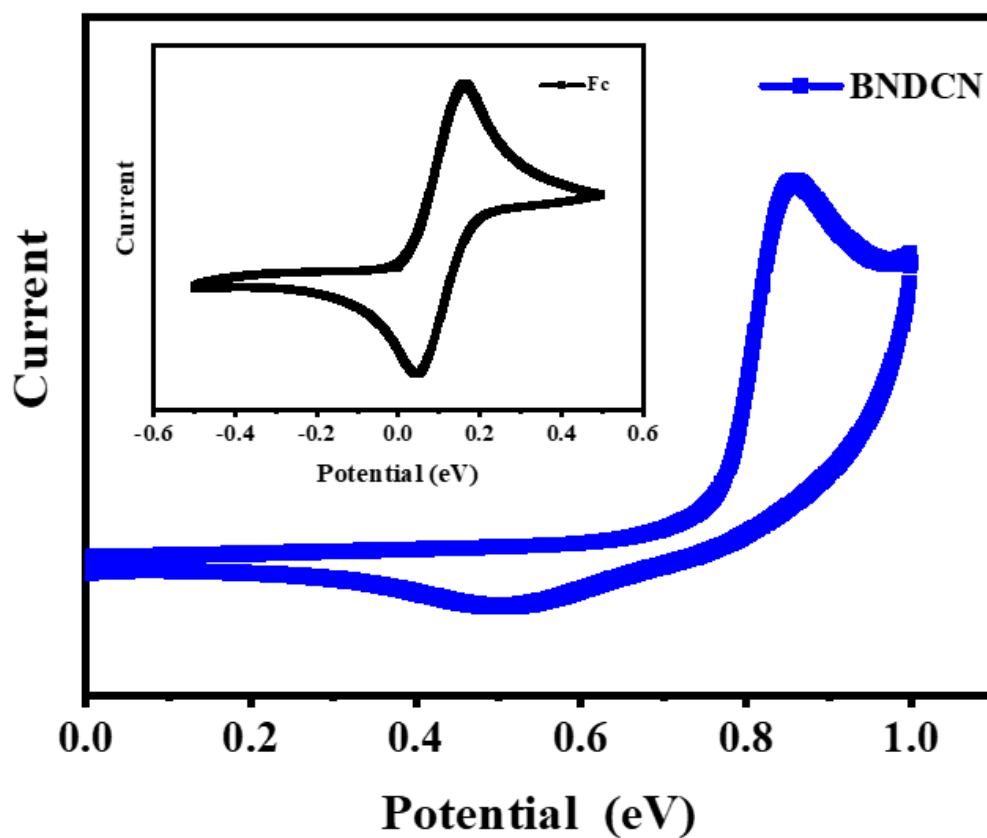


**Fig. S5** Cyclic voltammogram curves of BNDCN and ferrocene measured in CH<sub>3</sub>CN/DCM containing 0.1 M *tetra-n*-butylammonium hexafluorophosphate.

**Table S2.** Electrochemical properties of BNDCN.

Molecule	$E_{\text{ox,onset}}^{\text{a}}$ (V)	$E_{\text{g,opt}}^{\text{b}}$ (eV)	$E_{\text{HOMO}}^{\text{c}}$ (eV)	$E_{\text{LUMO}}^{\text{d}}$ (eV)
BNDCN	0.86	2.43	-5.50	-3.07

<sup>a</sup>The onset of oxidation curve; <sup>b</sup>Optical gap ( $1240/\lambda_{\text{onset}}$ ); <sup>c</sup> $E_{\text{HOMO}} = -[E_{\text{ox}} - E_{(\text{Fc}/\text{Fc}^+)} + 4.8]$  eV; <sup>d</sup> $E_{\text{LUMO}} = (E_{\text{HOMO}} + E_{\text{g,opt}})$ .

## 6. UV-vis absorption spectra simulations

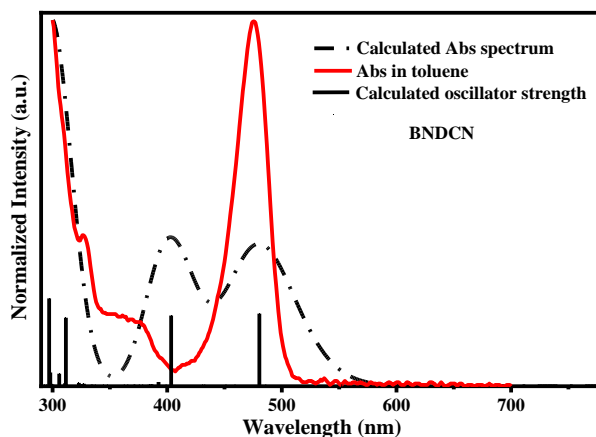
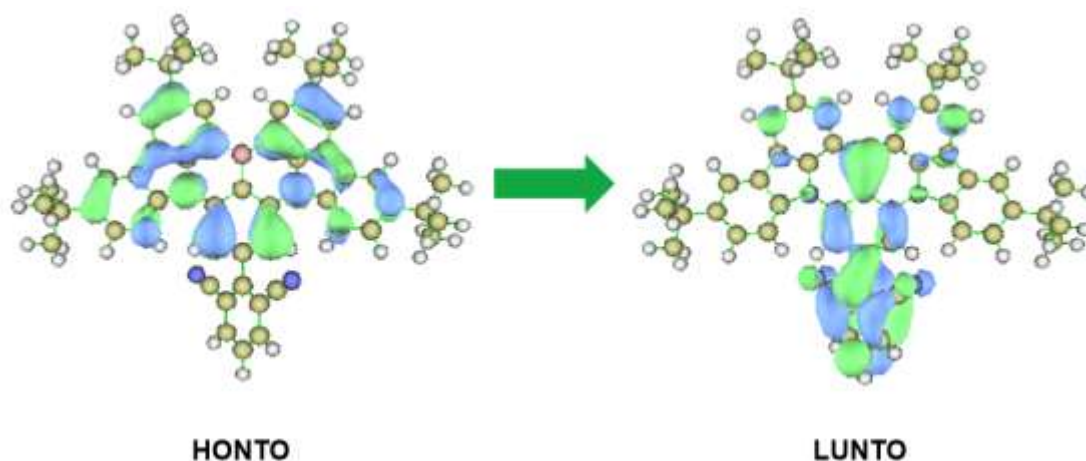


**Fig. S6** The calculated absorption spectra (dotted line), the experimentally measured absorption spectra (red line) and calculated oscillator strengths (black line) of BNDCN under TD-DFT based on B3LYP/6-31g(d,p) and generated calculated data processing through GaussSum-2.2.6.1 software.

**Table S3.** TD-DFT calculation results for BNDCN in the optimized  $S_0$  geometries at the B3LYP/6-31G(d,p) level.

compound	State	$E$ [eV]	$\lambda$ [nm]	$f$	Main configuration [%]
BNDCN	S <sub>1</sub>	2.57	483	0.0025	H→L 99
	S <sub>2</sub>	2.58	480	0.1982	H→L 99
	S <sub>3</sub>	3.08	403	0.1930	H→L+2 97
	S <sub>4</sub>	3.16	392	0.0116	H-1→L+1 98
	S <sub>5</sub>	3.21	386	0.0047	H-1→L 95
	S <sub>6</sub>	3.23	384	0.0040	H-2→L+1 95
	S <sub>7</sub>	3.26	380	0.0012	H-3→L+1 94
	S <sub>8</sub>	3.32	374	0.0003	H-2→L 93
	S <sub>9</sub>	3.34	370	0.0019	H-3→L 95



HONTO

LUNTO

Fig. S7 The natural transition orbital (NTO) analysis for  $S_1$  state of BND-CN.

## 7. Device characterization

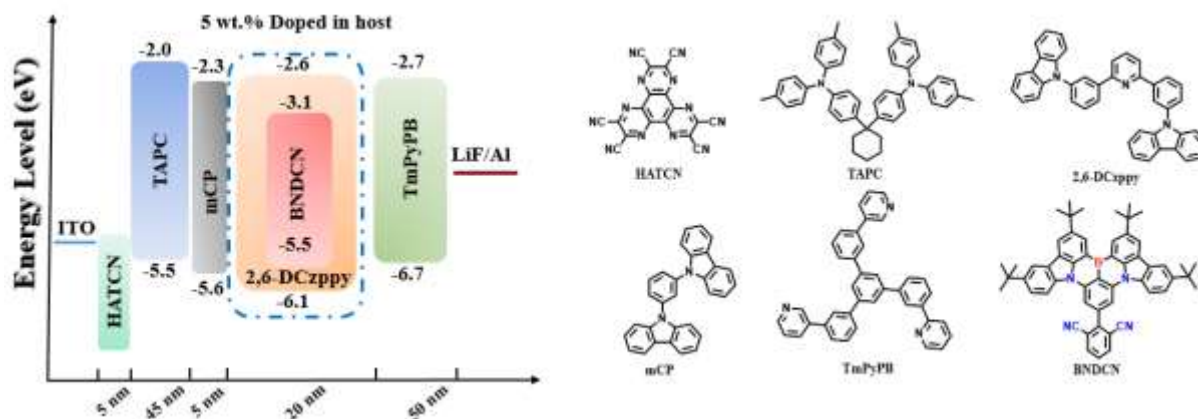


Fig. S8 The chemical structures of each functional layer materials and the corresponding OLED structures and energy diagrams.

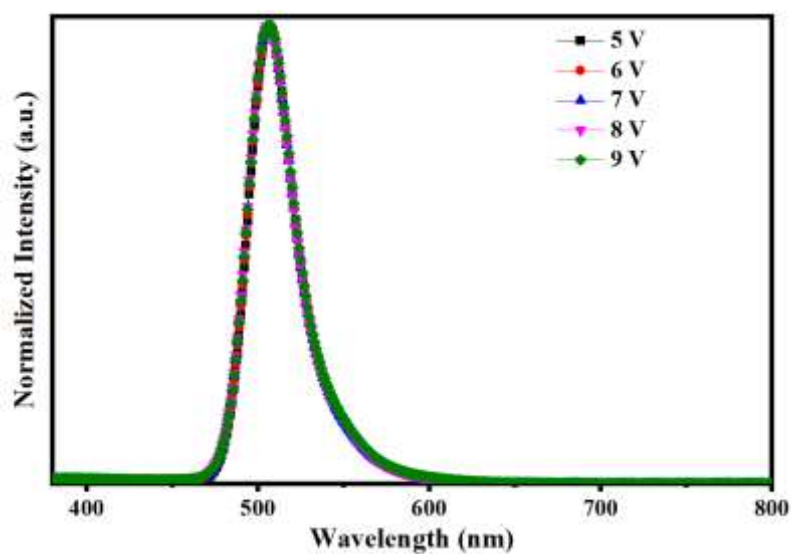


Fig. S9 EL spectra of BND-CN taken at various voltages from 5 to 9 V.



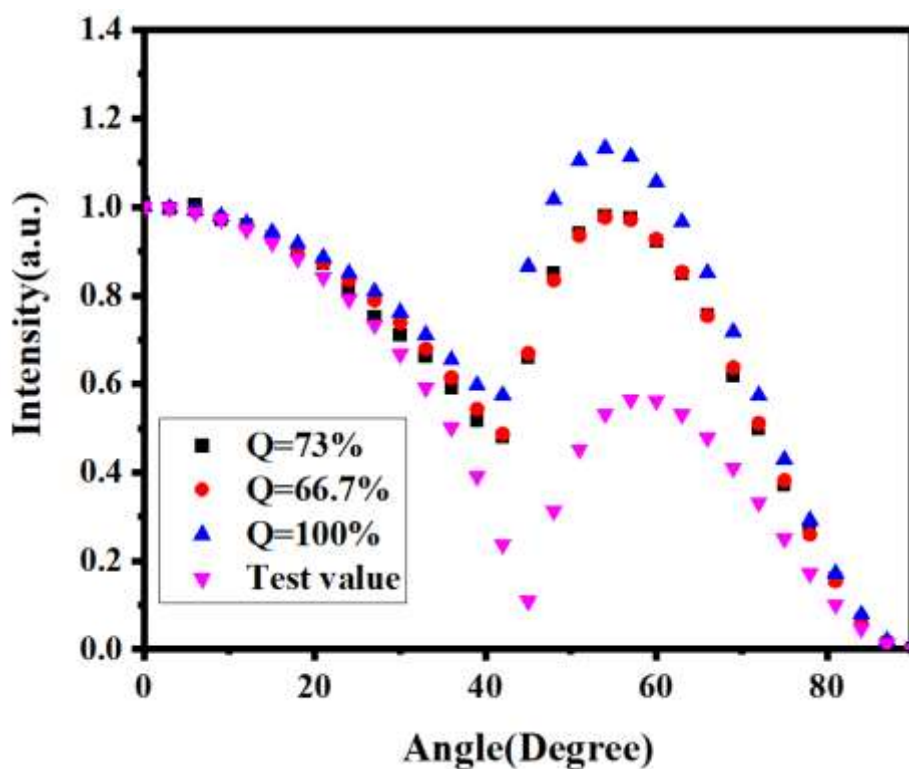


Fig. S10 Horizontal emitting dipole ratio of BNDCN in doped 2,6-DCzppy film (5 wt%).

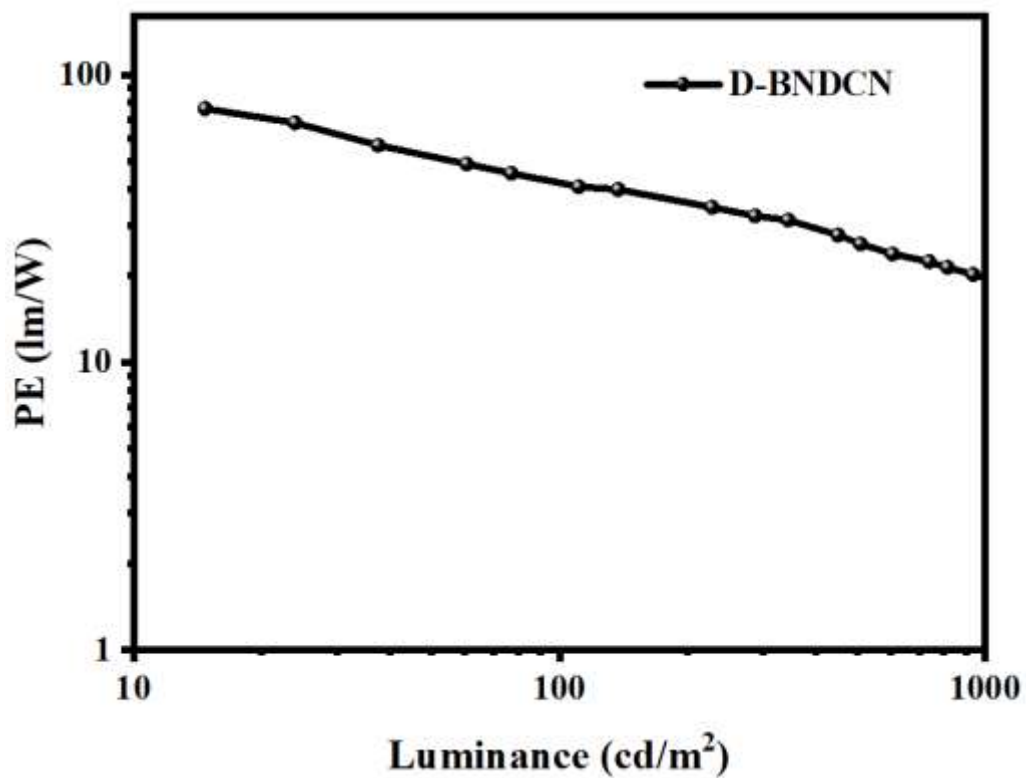
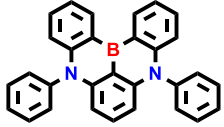
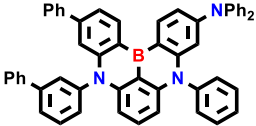
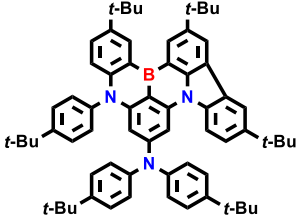
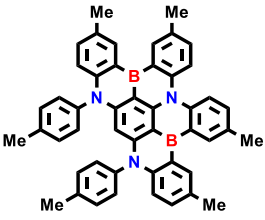
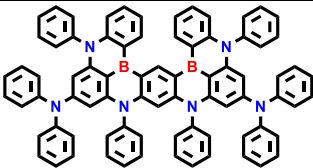
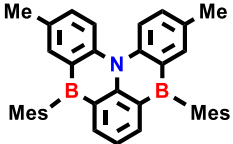
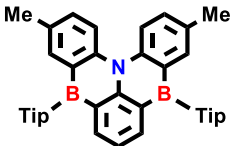
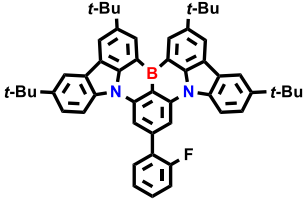
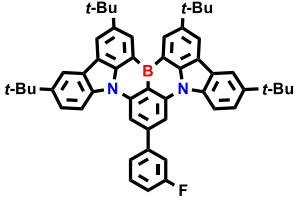
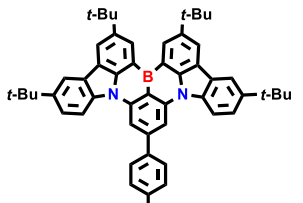
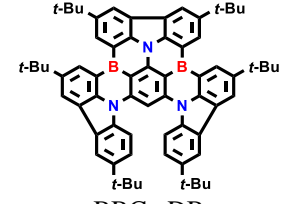
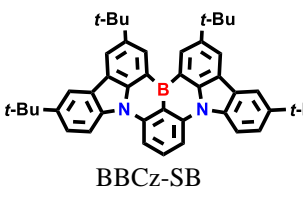
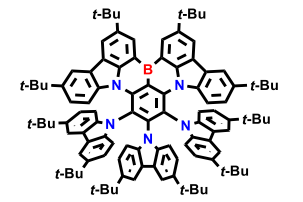
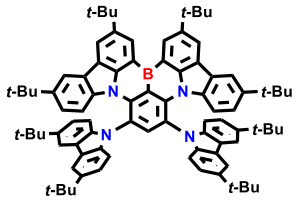
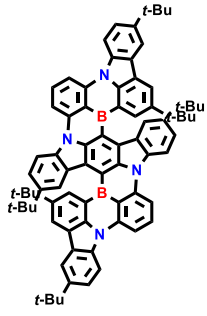
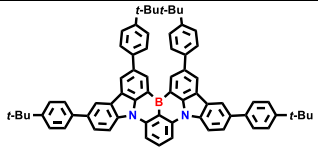
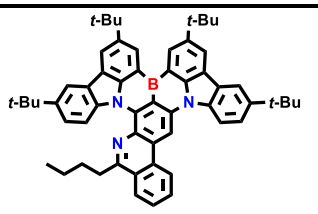
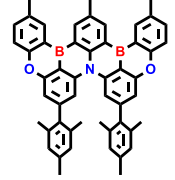
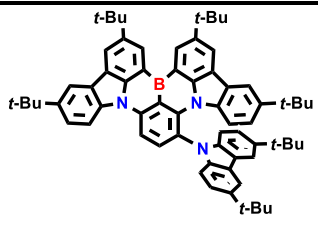
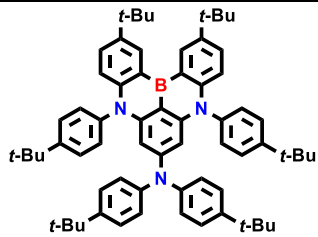


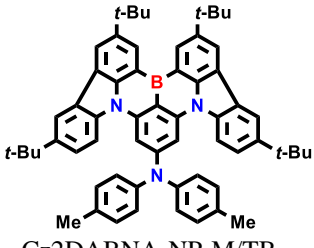
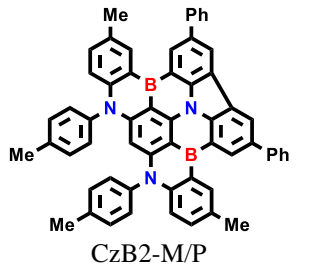
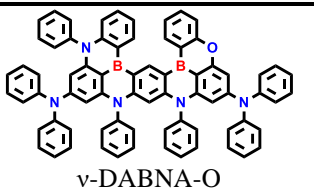
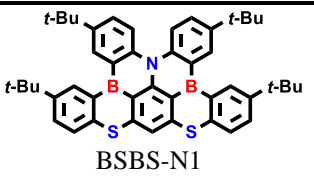
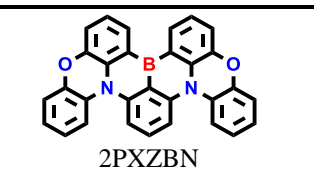
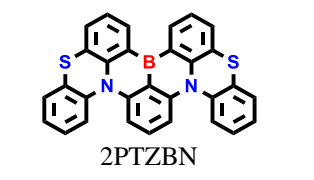
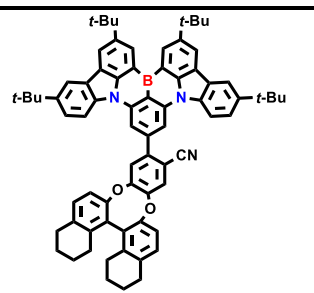
Fig. S11 PE-L curve of D-BNDCN.

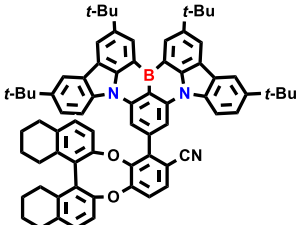
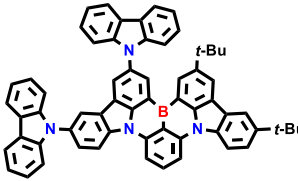
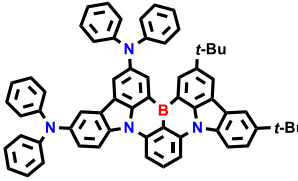
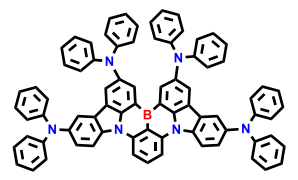
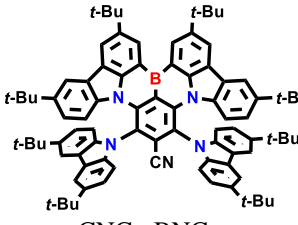
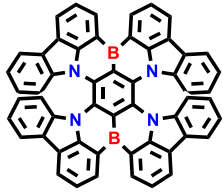
Table S4. The devices performances of representative NB-based MR-TADF-OLEDs vs this work.

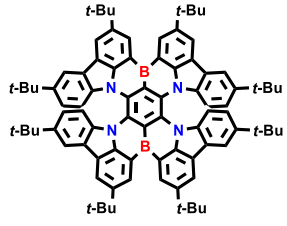
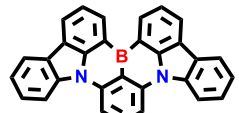
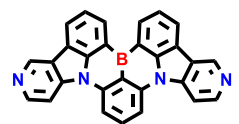
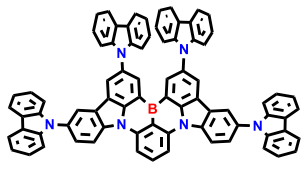
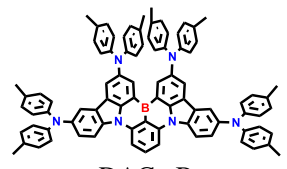
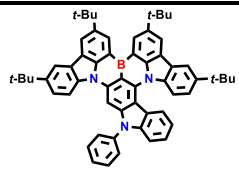
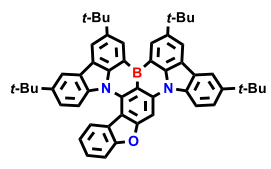
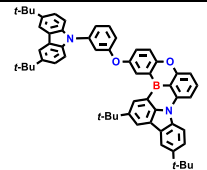
MR-TADF material	$\Delta E_{ST}^a$ [eV]	$k_{RISC}^b$ [ $10^5 \text{ s}^{-1}$ ]	FWHM <sup>c</sup> [nm]	$EQE_{max}$ [%]	Reference
 DABNA-1	0.15	0.10	28	13.5	<i>Adv. Mater.</i> <b>2016</b> , 28, 2777.
 DABNA-2	0.15	0.15	28	20.2	
 TBN-TPA	0.14	-	27	32.1	<i>Angew. Chem. Int. Ed.</i> <b>2018</b> , 57, 11316-11320
 B2	0.19	-	37	18.3	<i>J. Am. Chem. Soc.</i> <b>2018</b> , 140, 1195-1198
 v-DABNA	0.02	2.00	18	34.4	<i>Nat. Photonics</i> <b>2019</b> , 13, 678-682
 ADBNA-Me-Mes	0.18	0.08	32	24.5	<i>Org. Lett.</i> <b>2019</b> , 21, 9311-9314
 ADBNA-Me-Tip	0.18	0.09	33	34.7	

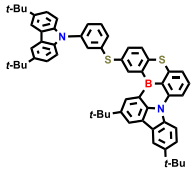
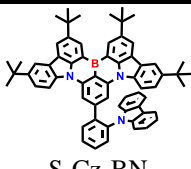
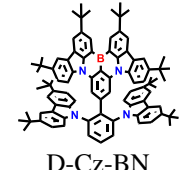
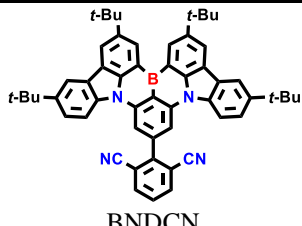
 <p>2F-BN</p>	0.16	0.22	40	22.0	
 <p>3F-BN</p>	0.08	0.39	39	22.7	<i>Angew. Chem. Int. Ed.</i> <b>2019</b> , <i>58</i> , 16912-16917
 <p>4F-BN</p>	0.11	0.44	32	20.9	
 <p>BBCz-DB</p>	0.15	0.22	27	29.3	<i>J. Am. Chem. Soc.</i> <b>2020</b> , <i>142</i> , 19468-19472
 <p>BBCz-SB</p>	0.15	0.20	26	27.8	
 <p>BBCz-G</p>	0.14	1.90	54	31.8	
 <p>BBCz-Y</p>	0.14	1.10	48	29.3	

 <p>BBCz-R</p>	0.19	0.12	26	22.0	
 <p>DtBuPhCzB</p>	0.09	-	33	25.5	<i>Adv. Opt. Mater.</i> <b>2020</b> , 8, 1902142
 <p>AZA-BN</p>	0.18	0.08	30	26.5	<i>Angew. Chem. Int. Ed.</i> <b>2020</b> , 59, 17499-17503
 <p>OAB-ABP-1</p>	0.12	0.40	33	21.8	<i>Adv. Mater.</i> <b>2020</b> , 32, 2004072
 <p><i>m</i>-Cz-BNCz</p>	0.08	10.0	45	31.4	<i>Angew. Chem. Int. Ed.</i> <b>2020</b> , 59, 17442-17446
 <p>DABNA-NP-TB</p>	0.17	0.14	33	26.7	<i>Angew. Chem. Int. Ed.</i> <b>2021</b> , 60, 2882-2886

 <p>Cz2DABNA-NP-M/TB</p>	0.14	0.73	27	21.8	
 <p>CzB2-M/P</p>	0.06	0.51	29	19.5	
 <p>v-DABNA-O</p>	0.03	1.60	23	29.5	<i>Angew. Chem. Int. Ed.</i> <b>2021</b> , <i>60</i> , 17910-17914
 <p>BSBS-N1</p>	0.13	19.00	25	21.0	<i>Angew. Chem. Int. Ed.</i> <b>2021</b> , <i>60</i> , 1-7
 <p>2PXZBN</p>	0.19	0.56	60	17.7	<i>Chem. Eng. J.</i> <b>2021</b> , <i>426</i> , 131169
 <p>2PTZBN</p>	0.15	1.17	58	25.5	
 <p>(R)-OBN-2CN-BN</p>	0.12	-	30	29.4	<i>Adv. Mater.</i> <b>2021</b> , <i>33</i> , 2100652

 <p>(R)-OBN-4CN-BN</p>	0.13	-	33	24.5	
 <p>BN1</p>	0.11	1.90	36	24.3	<i>Adv. Funct. Mater.</i> <b>2021</b> , <i>31</i> , 2102017
 <p>BN2</p>	0.13	1.50	46	24.5	
 <p>BN3</p>	0.09	1.40	43	24.7	
 <p>CNCz-BNCz</p>	0.18	4.20	49	33.7	<i>Chem. Sci.</i> <b>2021</b> , <i>12</i> , 9408-9412
 <p>R-BN</p>	0.18	0.67	48	25.6	<i>Angew. Chem. Int. Ed.</i> <b>2021</b> , <i>60</i> , 2-8

 <p>R-TBN</p>	0.16	0.25	49	24.7	
 <p>Cz-B</p>	0.14	0.20	30	22.6	<i>Angew. Chem. Int. Ed.</i> <b>2021</b> , <i>60</i> , 23142-23147
 <p><math>\gamma</math>-Cb-B</p>	0.12	0.58	28	19.0	
 <p>TCz-B</p>	0.09	0.13	30	29.2	
 <p>DACz-B</p>	0.14	0.10	44	19.6	
 <p>NBNP</p>	0.09	3.00	33	28.0	<i>Adv. Opt. Mater.</i> <b>2022</b> , <i>10</i> , 2102513
 <p>NBO</p>	0.12	9.30	29	26.1	
 <p>SBON</p>	0.16	0.50	28	13.7	<i>Adv. Opt. Mater.</i> <b>2022</b> , 2200504

 <p>SBSN</p>	0.10	1.5	31	17.6	
 <p>S-Cz-BN</p>	0.16	0.2	26	30.5	
 <p>D-Cz-BN</p>	0.14	0.2	24	37.2	
 <p>BNDCN</p>	0.06	0.8	30	32.3	This work

<sup>a</sup>Recorded in solution; <sup>b</sup>Recorded in doped film; <sup>c</sup>Recorded in device.